RSC Advances

ROYAL SOCIETY OF CHEMISTRY

www.rsc.org/advances

RSC Advances

RSCPublishing

ARTICLE

Highly efficient photoelectrochemical anticorrosion for 304 stainless steel by C_3N_4@ZnO composite with quasi-shell-core structure

Cite this: DOI: 10.1039/x0xx00000x

Received 00th January 2012,
Accepted 00th January 2012

DOI: 10.1039/x0xx00000x

www.rsc.org/

Yuyu Bu and Zhuoyuan Chen*

Carbon nitride@zinc oxide (C_3N_4@ZnO) composite with quasi-shell-core structure was prepared in this work. Coating C_3N_4 on ZnO significantly increases the photoelectrochemical anticorrosion performance of ZnO. When the C_3N_4 adding amount is 1 wt%, the C_3N_4@ZnO composite can provide the best photoelectrochemical anticorrosion capability for 304 stainless steel, and, this performance promotion is attributed to the formation of an effective heterojunction electric field on the interface between C_3N_4 and ZnO, which improves the separation efficiency of the photogenerated electron-hole pairs, increases the lifetime of the photoinduced electrons, and thus enhances the photoelectrochemcial anticorrosion performance of ZnO.

1. Introduction

Corrosion is inevitable since it is a decrease process of Gibbs free energy. Destructions carry out quietly due to corrosion. Corrosion will cause disastrous accidents without enough attention. Except for this, corrosion will induce a huge economic losses and cause serious environmental pollution. Although the currently existing technologies, such as organic coating and cathodic protection, can slow down the corrosion rates of metals, they cause a series of problems, such as material consumption, energy wastage, and environmental pollution. Therefore, new environment-friendly corrosion protection technologies must be developed.[1] Studies show that the photovoltaic effect of semiconductor materials with comparatively negative conduction band potentials can be used for the photoelectrochemical anticorrosion of metals. This novel technology is a very promising environment-friendly system, and it has been drawing increasing attention. The main advantage of this technology is to use clean and renewable solar energy for the corrosion protection of metals, and thus, it is considered to be an ideal corrosion protection technology and one of the most promising anticorrosion technologies. Solar energy is used to excite the semiconductor materials and generate photoinduced electrons due to the photovoltaic effect. The electrons subsequently migrate to and accumulate on the coupled metal surface. The potential of the metal will then be cathodically polarized and the anodic dissolution reactions of this metal are inhibited, thereby, the metal becomes cathodically protected. In contrast to the conventional sacrificial anodes in the cathodic protection system, semiconductor materials only act as photo-to-electron conversion centers and will not be consumed away. They can theoretically act as non-sacrificial photoanodes because the anodic reactions are not the decomposition of semiconductor materials themselves, but the oxidation of water and/or adsorbed organic pollutants by photogenerated holes.[2]

Recently, the investigations on photoelectrochemical anticorrosion are mainly focused on the wide bandgap semiconductor materials, such as TiO_2,[2-7] $SrTiO_3$,[8,9] and ZnO.[10] Studies show that the photoresponse of these materials can be extended to the visible light region by doping with other

nonmetallic or metallic elements or compositing with other narrow-bandgap semiconductor materials. In order to improve the photoelectric conversion performance, semiconductors with some special nanomorphologies, such as nanotube arrays, nanowires, and three-dimensional network structure, are prepared and studied.[11] To solve the continuity issue of anticorrosion in the dark at night, the semiconductor is composited with some materials possessing electronic storage capacity, such as WO_3,[12] SnO_2,[13] and CeO_2.[14] Studies show that these composites can continue the anticorrosion effect for stainless steel in the absence of light.

In a previous work,[15] graphitic carbon nitride (g-C_3N_4) was reported having great application potential in the areas of corrosion protection and photoelectrochemical anticorrosion because of its remarkable properties, such as good anti-abrasion and erosion properties, comparatively negative conduction band potential, visible light absorption, high performance price ratio, and simple film formation processes. However, core issues concerned about the wide application of g-C_3N_4 in photoelectrochemical anticorrosion are existed and need to be urgently solved. One of them is that the relatively low valence band potential (i. e., ~1.3 V vs NHE), which is slightly more positive than the oxidation potential of water (~1.229 V vs NHE), will result in a relatively lower oxidation capability and lead to a lower hole consumption rate. That means, the anodic depolarization process of the holes photoinduced by g-C_3N_4 will be very difficult to occur in the commonly used corrosion electrolyte system, for example 3.5% NaCl, where water is the only hole scavenger.[15] Therefore, in order to improve the applicability of g-C_3N_4 in the field of photoelectrochemical anticorrosion, g-C_3N_4 must be modified to increase the depolarization capability of the holes generated by g-C_3N_4 photoelectrode in the process of the photoelectrochemical reactions. Recently, the possible modification strategies mainly include the following aspects: compositing with other semiconductors that have more positive valence band potential; modifying g-C_3N_4 with other nanomaterials that can decrease the energy barrier of anodic depolarization reactions; positively shifting the valence band potential by doping methods.

ZnO has been widely studied in photoelectrochemical and photocatalytic areas. Compared with TiO_2, which was the first semiconductor material applied in photoelectric conversion, ZnO is both environment-friendly and inexpensive. The electron mobility of ZnO is about two orders of magnitude higher than that of TiO_2.[16] Thus, ZnO may have higher photoelectric conversion capability than TiO_2. Meanwhile, the conduction band potential of ZnO is more slightly negative than that of TiO_2, and as a result, the electrons photogenerated by ZnO can be easier to transfer to the coupled metal. Therefore, ZnO may be more advantageous than TiO_2 in the field of photoelectrochemical anticorrosion. It was reported that ZnO, composited with appropriate amount of π-conjugated material, such as polyaniline[17,18] and graphene,[19,20] can significantly increase the separation efficiency of the photogenerated electron-hole pairs due to the low electron transfer resistance in ZnO and the heterojunction electric field formed on the interface between them, thus significantly improving the photoelectric conversion ability of ZnO. g-C_3N_4 is a kind of π-conjugated material with graphite-like layered structure,[21] and the force between the layered structures of g-C_3N_4 is much smaller than that between the graphite layers. Thus, it is easy to disperse g-C_3N_4 to ultra-thin single layered structure by ultrasonic dispersion assisted method. Meanwhile, dispersed single-layer C_3N_4 can be very easy to assemble on the surfaces of other materials to form coating layers by intermolecular forces.[22] Pan et al.[23] prepared C_3N_4@$BiPO_4$ shell-core structured composite nanomaterial by ultrasonic dispersion assisted method and found that the photocatalytic performance was significantly improved. Zhang et al.[24] coated a C_3N_4 cladding layer on the surface of CdS nanowire and they found that the existence of this C_3N_4 cladding layer can significantly enhance the photocatalytic hydrogen production capability of CdS from water splitting.

Based on the above mentions, incorporating g-C_3N_4 and ZnO into nanocomposites is reasonable to anticipate a good photoelectrochemical anticorrosion performance. In this work, the carbon nitride@zinc oxide (C_3N_4@ZnO) composite with quasi-shell-core nanostructure was prepared by an ultrasonic dispersion assisted method and the photoelectrochemical anticorrosion performance of this composite was studied. Scanning electron microscope (SEM), high-resolution transmission electron microscope (HRTEM), X-ray diffraction (XRD), and X-ray photoelectron spectroscopy (XPS) were used to investigate the microstructures and the chemical compositions of this composite. UV/vis diffuse reflectance spectrum, photoinduced open circuit potential (OCP) variation, photoinduced current density, the photoinduced Volt-ampere characteristic curve (i-V curve), electrochemical impedance spectroscopy (EIS), and Mott-Schottky curve were performed to study the photoelectrochemical anticorrosion performance of this composite and to analyze the promotion mechanism of the photoelectrochemical anticorrosion performance of this composite.

2. Experimental

2.1 Preparation of mg-C_3N_4

The preparation of mg-C_3N_4 was based on the method used by Goettmann et al.[25] First, 1.2 g silicon dioxide (SiO_2) nanopowder with a diameter of approximately 15 nm was dispersed in 20 mL deionized water, and the resulting mixture was ultrasonically vibrated for 30 min. This dispersion liquid was added slowly to a dicyanodiamine solution prepared by dissolving 3 g dicyanodiamine in 20 mL deionized water. The liquid mixture was stirred in a 70 °C water bath until the water in the liquid mixture was completely evaporated. The dried powder was ground in an agate mortar, transferred to a crucible with a lid, and heated at 550 °C for 4 h at a heating rate of 20 °C min^{-1}. The light-yellow powder generated after sintering was added to 100 mL of 4 mol L^{-1} NH_4F solution and etched for 24 h. The powder was then filtered and repeatedly washed with deionized water. A yellow powder was obtained after drying at 80 °C for 4 h under vacuum conditions. All reagents used in this study were analytical ones from Aladdin Reagent Corporation.

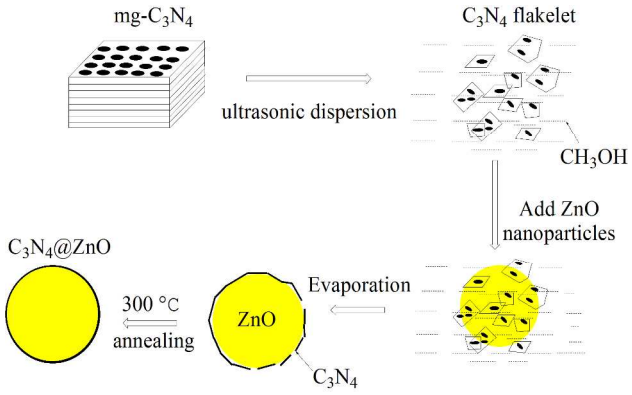

Scheme 1. Schematic illustration of the relevant preparation process of the C_3N_4@ZnO quasi-shell-core composite.

2.2 Preparation of C_3N_4@ZnO composite with quasi-shell-core structure

A certain amount of mg-C_3N_4 (accounting for 1, 2, 3 and 5 wt% of the mass of ZnO) was dispersed in 50 mL methanol, followed by sonication for 30 min. C_3N_4 flakelets were formed during the ultrasonic vibration of mg-C_3N_4. After that, 0.2 g ZnO particles, which were bought from Aladdin Reagent Corporation, was added into the mixture, followed by sonication for another 5 min. The resulting liquid mixture was then put in a hood and stirred until the completely evaporation of methanol in the liquid mixture. The C_3N_4@ZnO quasi-shell-core composite materials with different C_3N_4-adding ratios (1-5 wt%) were obtained after heating the dried powder at 300 °C for 30 min at a heating rate of 20 °C min^{-1}. The relevant preparation process is shown in Scheme 1.

2.3 Characterizations of the prepared C_3N_4@ZnO quasi-shell-core composite materials

The morphologies and the microstructure of the synthetic products were analyzed using a field emission SEM (Inspect F50, FEI Company, USA) and a HRTEM (Tecnai G2 F20, FEI Company, USA). The crystalline structures and bonding information of the synthetic products were analyzed using XRD

(D/MAX-2500/PC; Rigaku Co., Tokyo, Japan) and XPS (Axis Ultra, Kratos Analytical Ltd., England). The optical absorption properties were investigated using a UV/Vis diffuse reflectance spectrophotometer (U-41000; HITACHI, Tokyo, Japan).

2.4 Photoelectrode preparation

A fluorine-doped tin oxide (FTO) conductive glass (13 × 10 mm) was first ultrasonically cleaned with acetone of analytical grade for 5 min, rinsed with deionized water, and then dried with a clean, dry airflow. One longitudinal edge of the conductive side was then carefully covered with insulating tape, with the exposed effective area of the FTO glass measuring 1 cm^2. In total, 0.01 g as-prepared powder was mixed with 0.1 mL deionized water in an agate mortar, and the mixture was carefully ground for 10 min to form a homogeneous suspension. Then, 0.025 mL as-prepared suspension was evenly distributed onto the exposed area of the conductive side of the FTO glass. The insulating tape on the edge of the FTO glass was removed after the suspension had dried in the air. Finally, the FTO glass deposited with C_3N_4@ZnO powder was heated to 120 °C for 2 h under vacuum condition. A copper wire was connected to the conductive side of the FTO glass using conductive silver tape. Uncoated parts of the conductive side of the FTO glass were isolated with parafilm after the conductive silver tape had dried.

2.5 Electrochemical/Photoelectrochemical measurements

Electrochemical/photoelectrochemical measurements were performed using CHI660D Electrochemical Workstation (Shanghai Chenhua Instrument Co., Ltd., Shanghai, China). The prepared series C_3N_4@ZnO quasi-shell-core composite photoelectrodes, Ag/AgCl (saturated KCl), and Pt electrode acted as the working, reference, and counter electrodes, respectively. The potentials are reported on the Ag/AgCl (saturated KCl) scale. The schematic illustrations of the experimental setup for measuring the variations of the photoinduced OCP and current density, which were used to evaluate the photoelectrochemical anticorrosion performance of the prepared composites, were described in detail and shown in Figure 1 in a previous work from the authors' laboratory.[15] The variations of the photoinduced current density were measured at a 0 V bias potential, and the variations of the photoinduced OCP and current density were all measured under white light (250 mW cm^{-2}) illumination in 3.5 wt% NaCl at 25 °C. The white light, generated by a Xe arc lamp (PLS-SXE300, Beijing Changtuo Co. Ltd., Beijing, China), passed through a flat circular quartz window, equipped on the side of the three-electrode cell, and illuminated on the backside of the photoelectrode.

The i-V curves were measured from -0.8 V to 1.0 V with a scan rate of 0.02 $V \cdot s^{-1}$. The i-V curves, Mott-Schottky plots, and EIS tests were all performed in 0.1 mol L^{-1} Na_2SO_4 at 25 °C. Both Mott-Schottky plots and EIS tests were measured in the dark. EIS tests were performed at OCP over the frequency range between 10^4 and 10^{-1} Hz, with an AC voltage magnitude of 5 mV, using 12 points/decade. Mott-Schottky plots was measured at the potential range of -0.6 V ~ -0.1 V and the frequency of 10 Hz with an AC voltage magnitude of 10 mV. A three-electrode experimental system was employed to measure the i-V curves, Mott-Schottky plots, and EIS results.

3. Results and discussion

The surface morphologies of ZnO and C_3N_4@ZnO quasi-shell-core composites with different mg-C_3N_4 dosages (1% and 5%) were depicted in Figure 1. It was shown that the ZnO was existed as non-uniform short rods and most of them were approximately 1 μm in length and 500 nm in diameter (Figure 1a). For 1 wt% C_3N_4@ZnO quasi-shell-core composite (Figure 1b), ZnO particles turn to be more unclear and the surface turn to be much smoother compared to those shown in Figure 1a, demonstrating that C_3N_4 is covered on the surface of the ZnO nanoparticles. When the adding amount of C_3N_4 increases to 5 wt% (Figure 1c), ZnO particles are difficult to be distinguished, and the surface becomes smoother than those shown in Figure 1b, which may be caused by the coating of C_3N_4 on the surface

of ZnO particles. Furthermore, layered structure of C_3N_4 is not observed, as shown in Figures 1b and 1c, indicating that the

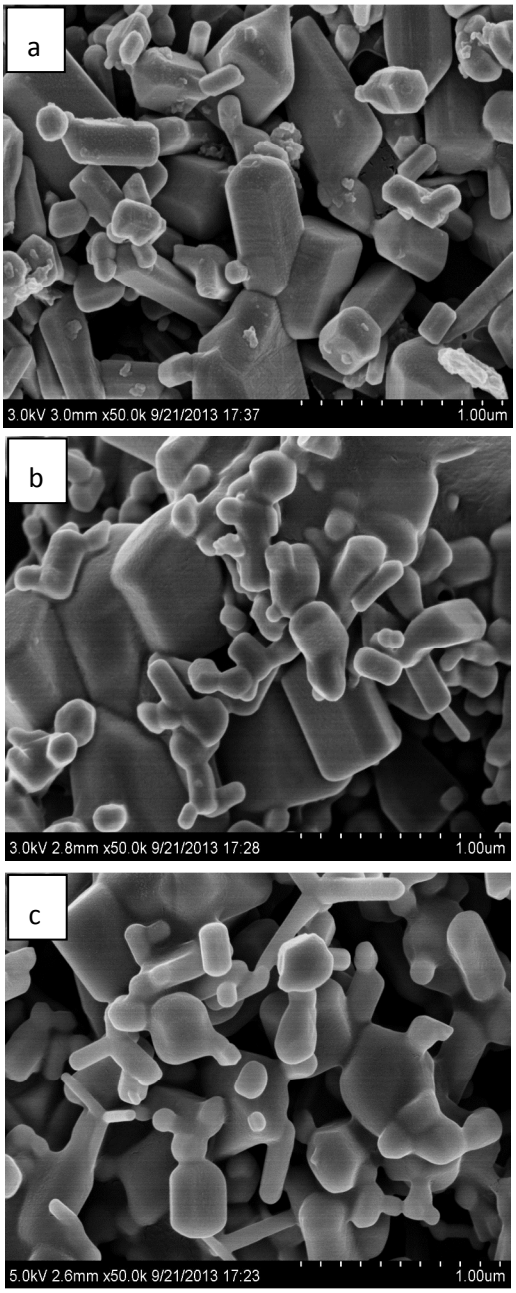

Figure 1. SEM images of (a) ZnO, (b) 1 wt% C_3N_4@ZnO quasi-shell-core composite and (c) 5 wt% C_3N_4@ZnO quasi-shell-core composite.

added C_3N_4 is dispersed to C_3N_4 flakelets with ultra-thin single layered structure by ultrasonic dispersion assisted method during the preparation process of the composite. Therefore, the composite prepared in this work can be expressed as C_3N_4@ZnO composites instead of mg-C_3N_4@ZnO composites, although the added carbon nitride materials are mg-C_3N_4.

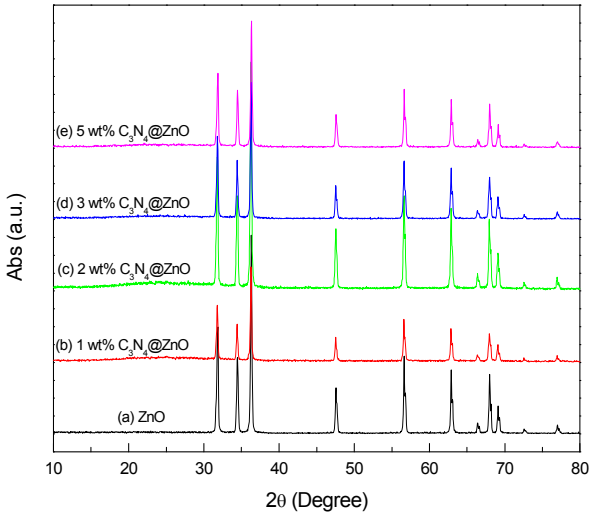

Figure 2. XRD patterns of (Curve a) ZnO, (Curve b) 1 wt% C_3N_4@ZnO quasi-shell-core composite, (Curve c) 2 wt% C_3N_4@ZnO quasi-shell-core composite, (Curve d) 3 wt% C_3N_4@ZnO quasi-shell-core composite and (Curve e) 5 wt% C_3N_4@ZnO quasi-shell-core composite.

Figure 2 shows the XRD patterns of ZnO and C_3N_4@ZnO quasi-shell-core composites with different mg-C_3N_4 dosages (1 %, 2 %, 3 % and 5 %). The diffraction peaks of commercial ZnO used in this work correspond to the standard lead-zinc ore structure. There is no significant difference between the diffraction peaks of the C_3N_4@ZnO quasi-shell-core composites and ZnO. For the C_3N_4@ZnO quasi-shell-core composites, a diffraction peak at $2\theta = 27.4°$ is expected, which is the characteristic index of the interlayer stacking of aromatic series for graphitic materials. However, this diffraction peak was not observed on the XRD patterns of the C_3N_4@ZnO quasi-shell-core composites, as shown in Curves 2b-2e in Figure 2. The absence of this diffraction peak can be caused by two reasons. One is that the adding amount of C_3N_4 in the composites is very little or the degree of crystallinity of C_3N_4 is not high enough. The other one is the disappearance of the layered structure of mg-C_3N_4 caused by ultrasonic dispersion.

In order to further study the C_3N_4 loading information on the ZnO surface, ZnO and C_3N_4@ZnO quasi-shell-core composites

with 1 and 5 wt% of mg-C_3N_4 were selected for HRTEM investigations. Figure 3a is the HRTEM image of ZnO, from which the ZnO (002) crystal plane can be clearly observed and the surface of ZnO is not adsorbed by other substance.

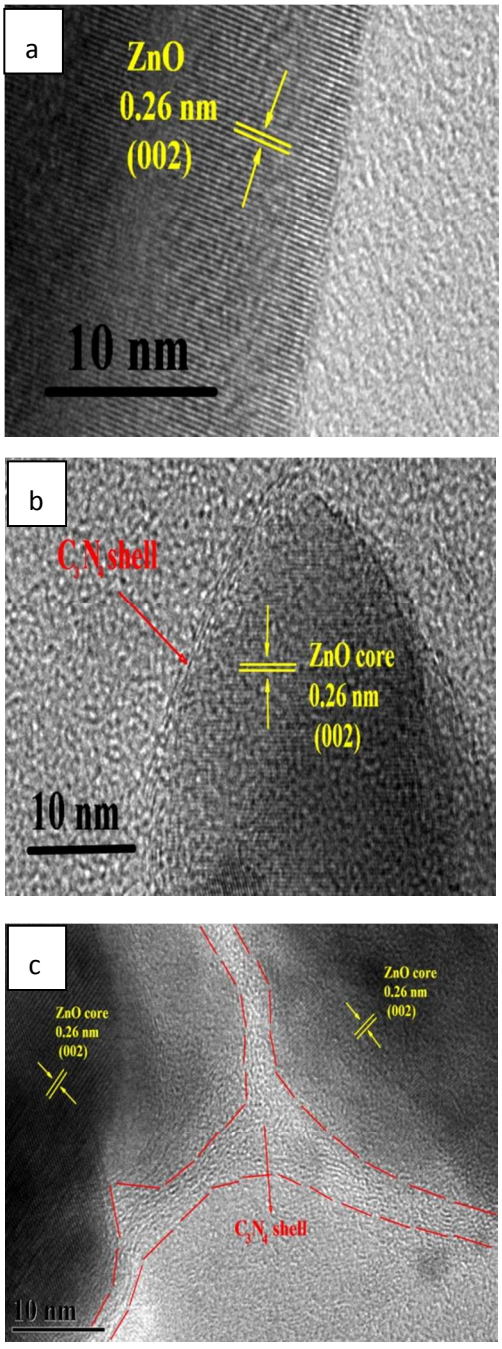

Figure 3. HRTEM images of (a) ZnO, (b) 1 wt% C_3N_4@ZnO quasi-shell-core composite and (c) 5 wt% C_3N_4@ZnO quasi-shell-core composite.

However, for 1 wt% C_3N_4@ZnO quasi-shell-core composite, a coating layer with the thickness of approximately 1 nm is observed on the surface of ZnO, as shown in Figure 3b. Meanwhile, the distinctness of ZnO (002) crystal plane is obviously declined, which can be attributed to the formation of C_3N_4 coating on the surface of ZnO. Figure 3c is the HRTEM result of 5 wt% C_3N_4@ZnO quasi-shell-core composite, from which a coating layer with the thickness of approximately 4 nm is observed on the surface of ZnO. The clarity of the ZnO (002) crystal plane is further declined compared with that shown in Figure 3b. The HRTEM results demonstrate that C_3N_4 was successfully coated on the surface of ZnO and the thickness of the coated C_3N_4 layer increases with the increase of the adding amount of mg-C_3N_4.

The chemical states of elements C and N of the coating layer on the ZnO surface were characterized using XPS and the relevant results of 1 wt% C_3N_4@ZnO quasi-shell-core composite were shown in Figure 4. Figure 4a shows the total survey spectrum. The binding energy peaks corresponding to Zn, O, C and N are observed in Figure 4a. Figure 4b shows the C1s XPS core level spectrum and the peak with the binding energy of 284.6 eV is the characteristic peak of C1s. Figure 4c shows the N1s XPS core level spectrum. Weak binding energy peak at 398.6 eV is observed, which is the characteristic peak of N1s. Compared with C1s, the characteristic peak of N1s at 398.6 eV is much weaker. The molar ratio of C to N in C_3N_4 is 3:4, thus, the difference of the intensities of these two peaks are expected to be little. In the present work, only 1 wt% C_3N_4 was coated on ZnO surface. In principle, the intensities of the characteristic peaks of both C1s and N1s should be very weak. However, the intensity of C1s peak is too much stronger than that of N1s, as shown in Figures 4b and 4c. The reason for causing this phenomenon may be due to the adsorption of CO_2 on 1 wt% C_3N_4@ZnO quasi-shell-core composite, resulting in the excessively high intensity of the C1s characteristic peak, as shown in Figure 4.

Figure 5 shows the UV/Vis diffuse reflectance spectra of ZnO and the C_3N_4@ZnO quasi-shell-core composites with different C_3N_4 dosages. The absorption band-edge of ZnO is

approximately 380 nm, as shown in curve 5a, which is consistent with the standard absorption threshold of ZnO.[26] After introducing C_3N_4, the absorption band-edge of the C_3N_4@ZnO quasi-shell-core composite red-shifts to >400 nm and the optical absorption intensity in the ultraviolet region at wavelength less than 380nm declines with the increase of the

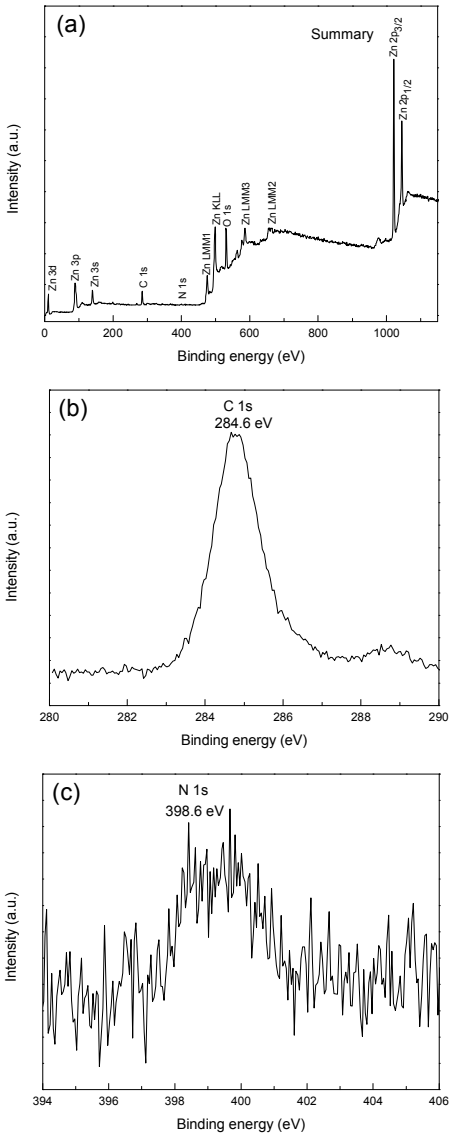

Figure 4. XPS spectra of 1 wt% C_3N_4@ZnO quasi-shell-core composite. Figure 4a shows the total survey spectrum. Figure 4b shows the C1s XPS core level spectrum. Figure 4c shows the N1s XPS core level spectrum.

adding amount of C_3N_4, indicating that C_3N_4 competes with ZnO on the absorption of the incident photons. The absorption capacity of the coated C_3N_4 is enhanced with the increase of the thickness of the coated C_3N_4 layer, leading to the gradual decrease of the absorption capacity of the C_3N_4@ZnO quasi-shell-core composites in the UV region.

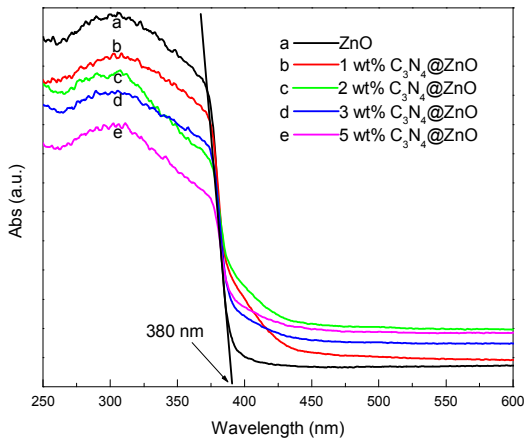

Figure 5. UV/Vis diffuse reflectance spectra of ZnO (Curve a); 1 wt% C_3N_4@ZnO quasi-shell-core composite (Curve b); 2 wt% C_3N_4@ZnO quasi-shell-core composite (Curve c); 3 wt% C_3N_4@ZnO quasi-shell-core composite (Curve d) and 5 wt% C_3N_4@ZnO quasi-shell-core composite (Curve e)

In order to study the effect of the coated C_3N_4 on the photoelectrochemical anticorrosion performance of ZnO, the OCP of C_3N_4@ZnO quasi-shell-core composites, 304 SS, and the mixed potentials of them were measured under intermittent white light on and off (Figure 6). As shown in curve 6a, the OCP of 304 SS electrode in 3.5 wt% NaCl solution is -0.09 V. After coupling with the ZnO thin-film photoelectrode in the dark, the mixed potential decreases to -0.17 V, as shown in Curve 6b. This can be ascribed to the more negative Fermi level of ZnO comparing with 304 SS. After coupling with the 1 wt% C_3N_4@ZnO quasi-shell-core composite thin-film photoelectrode in the dark, the mixed potential decreases to -0.20 V, as shown in Curve 6c. The OCP of 1 wt% C_3N_4@ZnO quasi-shell-core composite thin-film photoelectrode in the dark is -0.31 V, as shown in Curve 6g. After coupling 1 wt% C_3N_4@ZnO quasi-shell-core composite thin-film photoelectrode with 304 SS electrode in the dark, the mixed potential positively shifts to -0.20 V. As shown in Curves 6c-6e, the mixed potential of the couple of C_3N_4@ZnO quasi-shell-core composite thin-film photoelectrode with 304 SS

electrode in the dark decreases with the increase of the adding amount of C_3N_4. As we know, both C_3N_4 and ZnO are n-type semiconductors. C_3N_4 has a more negative conduction band potential and a more negative Fermi level potential than that of ZnO. After coating on the ZnO surface, C_3N_4 will pull the Fermi level potential of ZnO to negative direction, thus leading to the decrease of the OCP of the couple of the C_3N_4@ZnO quasi-shell-core composite thin-film photoelectrode with 304 SS electrode, and the shift value increases with the increase of the adding amount of C_3N_4. Under white light illumination, the OCP of the 304SS electrode coupled with C_3N_4@ZnO quasi-shell-core composite thin-film photoelectrode swiftly shifts to negative direction. After three cycles of white light on and off, the photoinduced OCP is stabilized. Table 1 shows the potential data obtained from Figure 6. E_1 is the stable potential of the 304SS electrode coupled with C_3N_4@ZnO quasi-shell-core composite thin-film photoelectrode after 100 seconds in dark condition. E_2 is the stable potential after 100 seconds light on at the third cycle of light on and off. ΔE stands for the potential drop caused by the white light illumination, which is the difference between E_2 and E_1. As shown in Table 1, E1 decreases with the increase of the adding proportion of C_3N_4 on ZnO in the dark, as discussed above. According to the data of the stable photoinduced potential, E_2, 1 wt% C_3N_4@ZnO quasi-shell-core composite thin-film photoelectrode can polarize the potential of 304 SS electrode to -0.40 V under white light illumination, which possess the optimum anticorrosion potential comparing with other adding proportions of C_3N_4 on ZnO. From the data of ΔE, 304 SS electrode coupled with 1 wt% C_3N_4@ZnO quasi-shell-core composite thin-film photoelectrode possesses the largest photoinduced potential drop, i. e., -0.21 V, and ΔE decreases with the increase of the adding amount of C_3N_4. The photoinduced potential drop is decreased to -0.04 V by increasing the adding amount of C_3N_4 to 5 wt%.

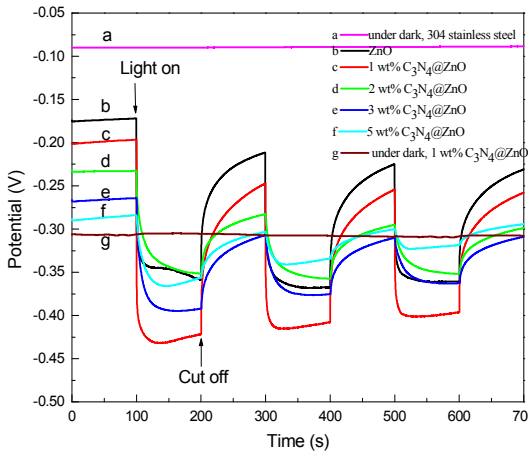

Figure 6. The open circuit potential of the Galvanic couple of 304 stainless steel with ZnO (Curve b); 1 wt% C_3N_4@ZnO quasi-shell-core composite (Curve c); 2 wt% C_3N_4@ZnO quasi-shell-core composite (Curve d); 3 wt% C_3N_4@ZnO quasi-shell-core composite (Curve e); 5 wt% C_3N_4@ZnO quasi-shell-core composite (Curve f) under intermittent white light on and off. Curve a is the open circuit potential of 304 stainless steel electrode and Curve g is that of 1 wt% C_3N_4@ZnO quasi-shell-core composite photoelectrode in the dark in 3.5 wt% NaCl solution..

Figure 7 shows the variations in the photoinduced current densities for the galvanic coupling between the ZnO or C_3N_4@ZnO quasi-shell-core composite thin-film photoelectrode and the 304 SS electrode under intermittent white light on and off. Positive excitation current densities are obtained under white light illumination. The C_3N_4@ZnO quasi-shell-core composite thin-film photoelectrode is connected to the working electrode interface of the potentiostat. Positive excitation currents show that the C_3N_4@ZnO quasi-shell-core composite thin-film electrode acts as an anode and generated anodic current, whereas the 304 SS electrode acts as a cathode and generated cathodic current. The generated anodic current indicates that the energies of the photoinduced electrons are high enough to overcome the energy barriers between the C_3N_4@ZnO quasi-shell-core composite thin-film photoelectrode and the 304 SS electrode. The photoinduced electrons can move toward the latter electrode to generate current, and the reduction of oxygen in the electrolyte on the interface between 304 SS and 3.5% NaCl can consume the photoinduced electrons but not those generated from the anodic

dissolution of 304 SS, indicating that the 304 SS is cathodically protected under white light irradiation. As shown in Figure 7, after three cycles of light on and off, the photoinduced current stabilizes gradually. The largest photoinduced current density is observed for the galvanic coupling between the 1 wt% C_3N_4@ZnO quasi-shell-core composite thin-film photoelectrode and the 304 SS electrode, indicating that the 1 wt% C_3N_4@ZnO quasi-shell-core composite thin-film photoelectrode can provide the best photoinduced anticorrosion for 304 SS. The photoinduced current density declines with the further increase of the adding amount of C_3N_4 in the C_3N_4@ZnO composites.

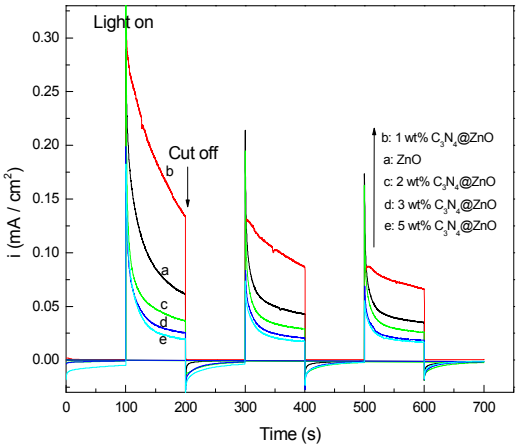

Figure 7. The variations in the current densities for the galvanic couple between 304 stainless steel electrode with ZnO (Curve a); 1 wt% C_3N_4@ZnO quasi-shell-core composite (Curve b); 2 wt% C_3N_4@ZnO quasi-shell-core composite (Curve c); 3 wt% C_3N_4@ZnO quasi-shell-core composite (Curve d); 5 wt% C_3N_4@ZnO quasi-shell-core composite (Curve e) thin-film photoelectrode under intermittent white light on and off in 3.5 wt% NaCl solution.

From the results shown in Figure 5, C_3N_4 competed with ZnO on the absorption of the incident photons, resulting in the decrease of the optical absorption of the C_3N_4@ZnO quasi-shell-core composites in the UV region. When the thickness of the C_3N_4 coating layer increases, the competitiveness of photon absorption by C_3N_4 is enhanced, resulting in the changes of its photoelectrochemical properties. As we know, the main issue of C_3N_4 in photoelectrochemical anticorrosion is that its intrinsic valence band potential is very negative, which makes the oxidizing capability of the photogenerated holes be very weak. In 3.5% NaCl solution, the photogenerated holes by C_3N_4 are difficult to oxidize the OH^- ionized from water, resulting in the impediment of the elimination process of the photogenerated holes. Therefore, the photoelectrochemical anticorrosion for 304 SS is difficult to be achieved. However, for 1 wt% C_3N_4@ZnO composite, the role of ZnO on the photon absorption is still dominant. Moreover, an efficient heterojunction electric field is formed between the interface of ZnO and C_3N_4, which can significantly improve the separation efficiency of the photogenerated electron-hole pairs, and hence can effectively promote its photoelectrochemical anticorrosion performance. The photoelectrochemical anticorrosion performance of C_3N_4@ZnO composites is determined by the C_3N_4 adding amount in the composite. When the C_3N_4 adding amount is low, the photogenerated holes by ZnO can transfer to the surface of C_3N_4 and react with water to eliminate them. Meanwhile, the photogenerated electrons can, through the incomplete coating area on the surface of ZnO, transfer to the nearby ZnO and finally to 304 SS. With the increase of the adding amount of C_3N_4, the incomplete coating area on the surface of ZnO may dramatically reduce, resulting in the increase of the difficulty for the electrons to transfer to 304 SS and making the photoelectrochemical anticorrosion performance decline to a certain extent. Considering the above discussed reasons, the photoelectrochemical anticorrosion performance of the 1 wt% C_3N_4@ZnO quasi-shell-core composite is the best.

In order to study the principle of the promotion of the photoelectrochemical properties of ZnO coated by 1 wt% C_3N_4, the i-V curve, EIS curve, and Mott-schottky curve were measured under the condition that 304 SS is not coupled with the 1 wt% C_3N_4@ZnO quasi-shell-core composite photoelectrode. Figure 8 shows the i-V curves of ZnO and series of C_3N_4@ZnO quasi-shell-core composite photoelectrodes. After the bias reaching -0.4 V, the photoinduced current increases quickly, and the maximum

photoinduced current is obtained with the bias of -0.2 V. Afterwards, with the further increase of the bias potential, the photoinduced current declines. Among these series photoelectrodes, the 1 wt% C_3N_4@ZnO quasi-shell-core composite photoelectrode has the largest photoinduced current, and excessive C_3N_4 will make the photoinduced current of C_3N_4@ZnO quasi-shell-core composite photoelectrode decline, as shown in Figure 8, demonstrating that 1 wt% C_3N_4@ZnO quasi-shell-core composite photoelectrode possess the best photoelectric conversion efficiency even without coupling with 304 SS.

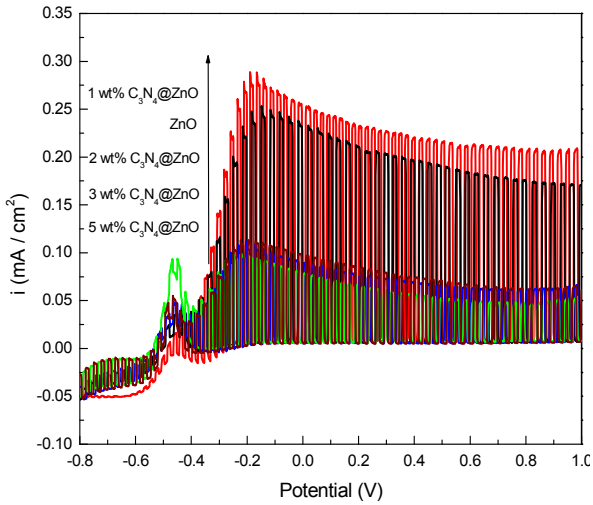

Figure 8. The photoinduced Volt-ampere characteristic curves of ZnO photoelectrodes; 1 wt% C_3N_4@ZnO quasi-shell-core composite; 2 wt% C_3N_4@ZnO quasi-shell-core composite; 3 wt% C_3N_4@ZnO quasi-shell-core composite; and 5 wt% C_3N_4@ZnO quasi-shell-core composite photoelectrodes in 0.1 M Na_2SO_4 solution.

Figure 9 shows the EIS results for the ZnO electrode, 1 wt% C_3N_4@ZnO and 5 wt% C_3N_4@ZnO quasi-shell-core composite photoelectrodes in the dark. The EIS results obtained from Figure 9 were fitted using the equivalent circuit inserted in the same figure. In this equivalent circuit, R_{sol} is the solution resistance; CPE is the constant phase angle element and its impedance is equal to $(Y_0(j\omega)^n)^{-1}$, where ω is the ac-voltage angular frequency (rad s^{-1}), and Y_0 and n are the frequency-independent parameters. R_T is the electron migration resistance in the thin-film photoelectrode, and the electron transfer and the reaction resistance on the interface between the semiconductor and the electrolyte. As shown in Figure 9, the measured data are represented by dots with different symbols, while, the solid lines are the fitted results using the provided equivalent circuit. The measured data are fitted very well. Table 2 lists the parameters of the EIS data. The R_T value obtained for ZnO is 2.79×10^5 Ω cm^2, which is approximately twice large than that for 1 wt% C_3N_4@ZnO composite, i. e., 1.33×10^5 Ω cm^2 (Table 2).While, the R_T value obtained for 5 wt% C_3N_4@ZnO composite is 2.10×10^5 Ω cm^2, which is located between those for ZnO and 1 wt% C_3N_4@ZnO composite. Because of the relatively low intrinsic electronic mobility in eigenstate C_3N_4, the electronic mobility of C_3N_4@ZnO composite, in principle, cannot benefit from the coating of C_3N_4 on ZnO. Therefore, it is considered that the decrease of the R_T value of 1 wt% C_3N_4@ZnO quasi-shell-core composite is mostly due to the formation of the heterojunction electric field on the interface between the ZnO and the coated C_3N_4, which will enhance the electron-hole separation efficiency and accelerate the interface reactions, and thus make the significant decrease of R_T. When the C_3N_4 adding amount is 5 wt%, the electron migration resistance in the thin-film photoelectrode increases again, indicating that the further increase of the thickness of the C_3N_4 coating layer will increase the electron migration resistance and hence decrease the photoelectrochemical performance of the C_3N_4@ZnO composite.

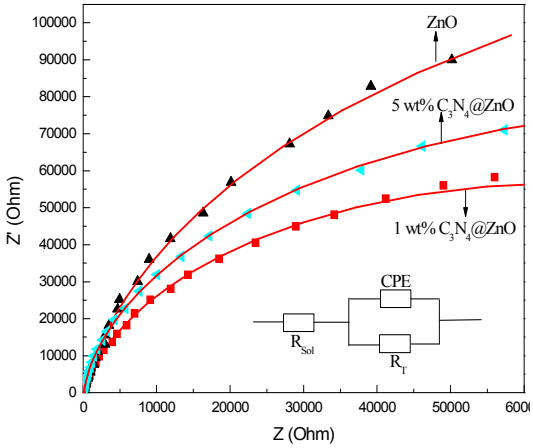

Figure 9. EIS spectra of the photoelectrodes prepared by ZnO, 1 wt% C_3N_4@ZnO and 5 wt% C_3N_4@ZnO quasi-shell-core

composite and the equivalent circuit for fitting the EIS results obtained in this work in 0.1 M Na_2SO_4 solution.

The conduction band potential and Fermi level potential of C_3N_4 are more negative than those of ZnO. Therefore, after coating with C_3N_4, ZnO is bound to cause the changes in energy level potential and thus a new interface electric field will be built on the interface between C_3N_4 and ZnO. In the present work, Mott-Schottky method was employed to study the relation between capacitance of the space charge region and the applied potential. The description of the specific formula is as follows:

$$1/C^2 = 2\,(e\varepsilon\varepsilon_0 N_D)^{-1} \cdot (E - E_{fb} - \kappa T/e) \quad (1)$$

where C is the capacitance of the space charge region in the semiconductor; N_D is the electron carrier density; e is the elemental charge; ε_0 is the permittivity of free space; ε is the relative permittivity of the semiconductor; E is the applied potential; E_{fb} is the flat band potential; T is the temperature; and κ is the Boltzmann constant.

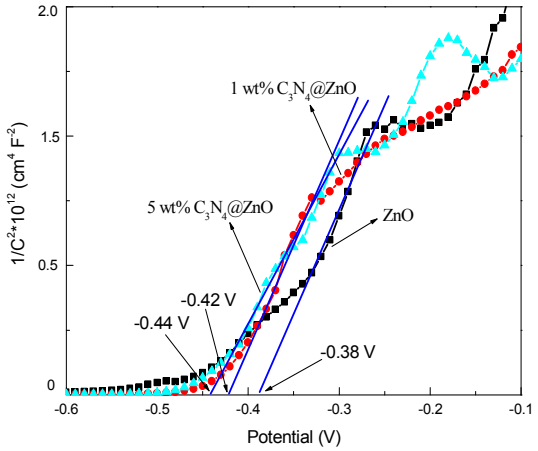

Figure 10. Mott-Schottky plots of ZnO, 1 wt% C_3N_4@ZnO and 5 wt% C_3N_4@ZnO quasi-shell-core composite photoelectrodes in 0.1 M Na_2SO_4 solution in the dark.

The flatband potential of a semiconductor material can be determined by extrapolating to $C^{-2} = 0$. The flatband potential of ZnO is approximately -0.38 V (Figure 10). After coating with 1 and 5 wt% C_3N_4, the flatband potentials of the C_3N_4@ZnO composites are negatively shifted to -0.42 and -0.44 V (Figure 10), respectively, indicating that trace C_3N_4 causes the negative shift of the flatband potentials of ZnO and the negative shift value increases with the increase of the C_3N_4 adding amount in the C_3N_4@ZnO composites. This change trend is consistent with that of the OCPs at the first 100 s in the dark shown in Figure 6, from which the OCPs of the C_3N_4@ZnO composites shift to negative direction with the increase of the C_3N_4 adding amount. Because the Fermi level potential of C_3N_4 is more negative than that of ZnO, the new Fermi level of 1 wt% C_3N_4@ZnO composite will located between those of C_3N_4 and ZnO after coating C_3N_4 on ZnO surface. The negative shift of the Fermi level of ZnO will induce the negative shift of the conduction band potential of ZnO,[27] which will, therefore, increase the reduction capability of the photogenerated electrons, thus improves its photoelectrochemical anticorrosion performance to some extent. Meanwhile, the movement of the Fermi level will lead to the directional migration of electrons and thus the formation of electrical field on the interfaces. Under white light illumination, this interface electric filed can increase the separation efficiency of the photogenerated electron-hole pairs and the lifetime of the photogenerated electrons, therefore making the photoelectrochemical anticorrosion performance of C_3N_4@ZnO composite be higher than that of ZnO.

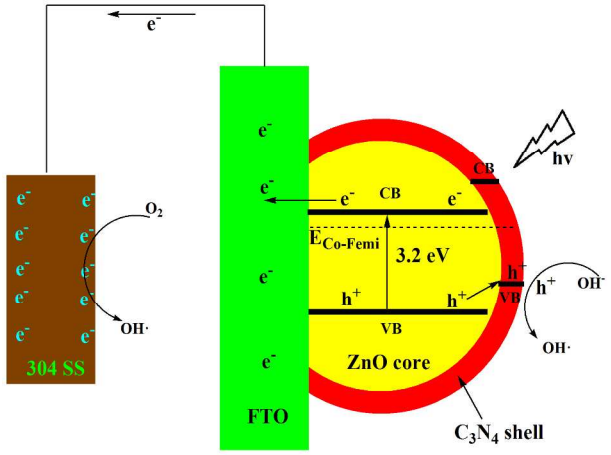

Figure 11. Proposed mechanism for the promotion of the photoelectrochemical anticorrosion performance for 304 stainless steel by 1 wt% C_3N_4@ZnO quasi-shell-core composite.

Figure 11 schematically shows the proposed mechanism for the promotion of the photoelectrochemical anticorrosion performance for 304 SS by 1 wt% C_3N_4@ZnO quasi-shell-core composite. After coating 1 wt% C_3N_4 on ZnO surface, the thickness of the C_3N_4 coating layer is approximately 1 nm and C_3N_4 is not the major photo absorption material in this composite. The photo absorption is still mainly from that of ZnO. ZnO absorbs the light with the wavelength less than 380 nm and generates photoinduced electrons and holes. The difference in Fermi levels between ZnO and C_3N_4 results in the formation of a heterojunction electric field on the interface between these two phases. Usually, the movement of Fermi level will lead to the bending of the energy bands of these two semiconductors. However, the thickness of the C_3N_4 coating layer is only 1 nm, which is much smaller than that of the depletion layer of the semiconductor. The valence band of C_3N_4 remains flat band state since it cannot form an effective energy band bending. The photogenerated electrons on the conduction band of ZnO will move to the FTO glass and will finally transfer to the coupled 304 SS and provide an effective cathodic protection for it. The photogenerated holes left on the valence band of ZnO will transfer to the valence band of C_3N_4 and participate in the oxidation process on the surface of C_3N_4. Therefore, coating a small amount of C_3N_4 on ZnO surface can increase the separation efficiency of the photogenerated electrons and holes and thus improve the photoelectrochemical anticorrosion performance of ZnO. On the other hand, coating C_3N_4 on ZnO surface can improve the surface state of ZnO and make this C_3N_4@ZnO quasi-shell-core composite much more easily connect with other organic coatings, further enhancing its potential for practical application.

Table 1. The photoinduced open circuit potential variations of ZnO and series C_3N_4@ZnO quasi-shell-core composite photoelectrodes.

	ZnO	1 wt% C_3N_4@ZnO	2 wt% C_3N_4@ZnO	3 wt% C_3N_4@ZnO	5 wt% C_3N_4@ZnO
E_1 (V)	-0.17	-0.19	-0.23	-0.26	-0.28
E_2 (V)	-0.36	-0.40	-0.35	-0.36	-0.32
ΔE (V)	-0.19	-0.21	-0.12	-0.10	-0.04

Table 2. Fitted parameters of the EIS of ZnO, 1 wt% C_3N_4@ZnO and 5 wt% C_3N_4@ZnO quasi-shell-core composite photoelectrodes in 0.1 M Na_2SO_4 solution in the dark.

Samples	R_{Sol} (Ω cm^2)	n	CPE (Ω^{-1} cm^2 s^n)	R_T (Ω cm^2)
ZnO	32.10	0.92	1.17×10^{-5}	2.79×10^{5}
1 wt% C_3N_4@ZnO	28.80	0.90	1.18×10^{-5}	1.33×10^{5}
5 wt% C_3N_4@ZnO	29.30	0.91	1.19×10^{-5}	2.10×10^{5}

4. Conclusion

The C_3N_4@ZnO composite with quasi-shell-core structure was successfully prepared in this work and it can provide the best photoelectrochemical anticorrosion capability for 304 stainless steel when the C_3N_4 adding amount is 1 wt%. With the further increase of the C_3N_4 adding amount, the photoelectrochemical anticorrosion capability of the C_3N_4@ZnO composite with quasi-shell-core structure declines. According to the experimental results from UV/Vis diffuse reflectance spectra, i-V curves, electrochemical impedance spectra and Mott-Schottky plots, an ultrathin coating layer of C_3N_4 on the surface of ZnO helps to form a heterojunction electric field on the interface between C_3N_4 and ZnO, thereby enhancing the separation efficiency of the photogenerated electron-hole pairs. However, excessive C_3N_4 will compete with ZnO on the absorption of photons, and the photoelectrochemical anticorrosion performance of this composite will significantly decline when C_3N_4 becomes the principal photon absorber. Meanwhile, overly thick C_3N_4 cladding layer will increase the charge transfer resistance, and thus lower down the

photoelectrochemical anticorrosion performance of this composite to some extent.

Acknowledgements

This work was financially supported by the National Natural Science Foundation of China (Grant No. 41376126) and the Hundreds-Talent Program of the Chinese Academy of Sciences (Y02616101L).

Notes and references

Key Laboratory of Marine Environmental Corrosion and Bio-fouling, Institute of Oceanology, Chinese Academy of Sciences, 7 Nanhai Road, Qingdao 266071, China.

*Corresponding author, Prof. Zhuoyuan Chen; Email: zychen@qdio.ac.cn; Tel: +86-532-82898731; Fax: +86-532-82880498

1 B.A. Shaw and R.G. Kelly, *Electrochem. Soc. interface*, 2006, 24-26.

2 Y. Ohko, S. Saitoh, T. Tatsuma, and A. Fujishima, *J. Electrochem. Soc.* 2001, **148**, B24-B28.

3 H.W. Park, K.Y. Kim and W.Y. Choi, *J. Phys. Chem. B*, 2002, **106**, 4775-4781.

4 C. Lei, Y. Liu, H. Zhou, Z. Feng and R. Du, *Corros. Sci.*, 2013, **68**, 214-222.

5 Z. Q. Lin, Y. K. Lai, R. G. Hu, J. Li, R. G. Du and C. J. Lin, *Electrochim. Acta*, 2010, **55**, 8717-8723.

6 S. Li and J. Fu, *Corros. Sci.*, 2013, **68**, 101-110.

7 S. Li, Q. Wang, T. Chen, Z. Zhou, Y. Wang and J. Fu, *Nanoscale Res. Lett.*, 2012, **7**, 227.

8 Y. Ohko, S. Saitoh and T. Tatsuma, A. Fujishima, *Electrochem. Solid-State Lett.*, 2002, **5**, B9-B12.

9 Y. Y. Bu, W. B. Li, J. Q. Yu, X. T. Wang, M. L. Qi, M. Y. Nie and B. R. Hou, *Acta Phys-Chim Sin.*, 2011, **27**, 2393-2399.

10 M. M. Sun, Z. Y. Chen, Y. Y. Bu, J. Q. Yu and B. R. Hou, *Corros. Sci.*, 2014, **82**, 77-84.

11 Y. F. Zhu, R. G. Du, W. Chen, H. Q. Qi and C. J. Lin, *Electrochem. Commun.*, 2010, **12**, 1626-1629.

12 T. Tatsuma, S. Saitoh, Y. Ohko and A. Fujishima, *Chem. Mater.*, 2001, **13**, 2838-2842.

13 R. Subasri and T. Shinohara, *Electrochem. Commun.*, 2003, **5**, 897-902.

14 R. Subasri, S. Deshpande, S. Seal and T. Shinohara, *Electrochem. Solid-State Lett.*, 2006, **9**, B1-B4.

15 Y. Y. Bu, Z. Y. Chen, J. Q. Yu and W. B. Li, *Electrochim. Acta*, 2013, **88**, 294-300.

16 H. Pan, N. Misra, S.H. Ko, C.P. Grigoropoulos, N. Miller, E.E. Haller and O. Dubon, *Appl. Phys. A: Mater. Sci. Process.*, 2009, **94**, 111-115.

17 V. Eskizeybek, F. Sari, H. Gulce, A. Gulce and A. Avci, *Appl. Catal., B*, 2012, **119**, 197-206.

18 J. Singh, A.P. Bhondkar, M.L. Singla and A. Sharma, *ACS Appl. Mater., Interface*, 2013, **5**, 5346-5357.

19 T. Xu, L. Zhang, H. Cheng and Y. Zhu, *Appl. Catal., B*, 2011, **101**, 382-387.

20 Y. Y. Bu, Z. Y. Chen, W. B. Li and B. R. Hou, *ACS Appl. Mater. Interface*, 2013, **5**, 12361-12368.

21 X. C. Wang, K. Maeda, A. Thomas, K. Takanabe, G. Xin, J. M. Carlsson, K. Domen and M. Antonietti, *Nat. Mater.*, 2009, **8**, 76-80.

22 X. Zhang, X. Xie, H. Wang, J. Zhang, B. Pan and Y. Xie, *J. Am. Chem. Soc.*, 2013, **135**, 18-21.

23 C. Pan , J. Xu , Y. Wang , D. Li and Y. Zhu, *Adv. Funct. Mater.*, 2012, **22**, 1518-1524.

24 J. Zhang, Y. Wang, J. Jin, J. Zhang, Z. Lin, F. Huang and J. Yu, *ACS Appl. Mater. Interface*, 2013, **5**, 10317-10324.

25 F. Goettmann, A. Fischer, M. Antonietti and A. Thomas, *Angew. Chem.-Int. Edit.*, 2006, **45**, 4467-4471.

26 A. Steinfeld, *Inter. J. Hydro. Energy*, 2002, **27**, 611-619.

27 Z. Zhang and J. T. Yates, *Chem. Rev.*, 2012, **112**, 5520-5551.